nucleus is either B^{12} or N^{12} in a particle-stable state. (These reactions are kinematically distinguishable, and would lead to a bump on the rising edge of the differential cross-sections in Figs. 10–12). From the data we can say that these processes therefore amount to less than about 10% of the total pion photoproduction cross-section from carbon at 200 Mev photon energy.

ACKNOWLEDGMENTS

We wish to recognize here the assistance of Professor H. R. Fechter in several phases of the experiment. Mr. R. Fessel developed much of the electronics used and aided in numerous other ways. Mr. D. Johnson and the synchrotron crew provided steady beams and assisted in taking data.

PHYSICAL REVIEW VOLUME 122, NUMBER 4 MAY 15, 1961

Comparison of the Scattering of Positrons and Electrons from Nuclear Charge Distributions*

GEORGE H. RAWITSCHER
Yale University, New Haven, Connecticut

AND

C. RUTHERFORD FISCHER
New Mexico State University, Las Cruces, New Mexico

(Received January 3, 1961)

Elastic scattering cross sections of 183-Mev positrons and electrons are calculated for various charge distributions of the Ca and Au nuclei. It is shown that the combined use of positron and electron scattering measurements can lead to a determination of the nuclear charge distribution which is more accurate than that derived from either one of the scattering cross sections when used by itself. The scattered particles obey Dirac's equation and the nuclei are assumed to be static spherically symmetric charge distributions, whose radial dependence is given in terms of a three-parameter family of curves.

I. INTRODUCTION

A GREAT deal of information concerning the dependence of nuclear charge density on radial distance has been achieved in the last years,[1] in particular by the high-energy electron scattering experiments.[2] The charge density is determined with highest accuracy at the nuclear surface, near the "halfway point," a certain amount of ambiguity still remaining at the central and tail regions. Positrons may prove useful in resolving such uncertainties because, due to repulsion rather than attraction of the wave function from the center of the nucleus, the different regions of the nuclear charge distribution should affect the cross section with weights differing from those in the case of electrons.[3]

This work is an attempt to establish the nature and extent of such positron-electron differences in a rough exploratory fashion. Cross sections of positrons and electrons scattered by nuclei having various spherical charge distributions are calculated numerically. The radial dependence of the nuclear charge distributions considered in this work is given in terms of three parameters and can be made to vary continuously from a "wine-bottle" to a Woods-Saxon form. The effect on the electron scattering cross section produced by a change in the form of the nuclear charge distribution is compared to the corresponding effect on the positron cross section. Conclusions are drawn regarding the reduction of the inaccuracy in the determination of the charge distribution from the combined e^+ and e^- scattering experiments and analyses. Incidentally, refinement of this type of investigation might ultimately permit the detection of effects which are usually neglected in the calculations, for instance, the deformation from sphericity which could occur during the scattering.

In Sec. III a comparison between the electron and positron cross sections is made for four shapes of the charge distribution of Ca. Two of the charge distributions (WB–1 and WB–2) have various central wine-bottle-like depressions, and are intended to furnish a comparison of sensitivity of electron and positron scattering to the internal regions of the nucleus. The two other charge distributions (WS–1 and WS–2) have no central depression but differ instead by 6% in their surface thickness. The nucleus chosen is Ca because in this case the numerical inaccuracies in the cross section are estimated to be small compared to the effect due to the changes of the charge distribution.

Two other charge distributions are considered for the nucleus of Au. The effects are sizable in this case, but

* This research was supported by the U. S. Air Force under a contract monitored by the Air Force Office of Scientific Research of the Air Research and Development Command.

[1] K. W. Ford and D. L. Hill, Ann. Rev. Nuclear Sci. **5**, 25 (1955).

[2] R. Hofstadter, Ann. Rev. Nuclear Sci. **7**, 231 (1957).

[3] The authors are indebted to Professor G. Breit for bringing this point to their attention. Compare also with footnote 12.

the accuracy of the calculation, as discussed in Sec. IV, is smaller than in the case of Ca. A list of some of the notations used in what follows is given below.

$\kappa=p/\hbar$, where $\hbar$ is Planck's constant divided by 2π, and p the momentum of the incident particle.

$x=\kappa r$, where r is the radial distance from the center of the nucleus.

$x_0=\kappa r_0$, the matching radius.

$Z\alpha=\pm Ze^2/\hbar c$. The upper sign refers to electrons, the lower one to positrons. The atomic number of target nucleus is Z.

$\beta=v/c$, where v is the velocity of the incident particle.

$\eta=-\alpha/\beta$.

k=eigenvalue of angular momentum operator $\rho_3[\mathbf{L}\cdot\boldsymbol{\sigma}+1]$ as defined for instance in the work cited in footnote 10. The values are ±1, ±2, etc.

R and I superscripts denote quantities occurring in the calculation of the regular and irregular Coulomb wave functions.

$G_k(x)$ and $F_k(x)$ are nuclear wave functions defined in Eqs. (A1) and (A2) of the Appendix.

δ_k are the nuclear phase shifts defined in Eq. (A3′).

z, c, and w are the three parameters which determine the shape of the nuclear charge distribution as given by Eq. (1).

WS denotes a charge distribution of Woods-Saxon form, given by Eq. (1) with $w=0$.

WB denotes a charge distribution of a wine-bottle form, given by Eq. (1) when $w\neq0$.

II. METHOD

Since analytic approximations are unreliable in the high-energy region for nuclei of large atomic number Z, the work is carried out numerically in a similar spirit to that of Hahn, Ravenhall, and Hofstadter.[4] The potential responsible for the scattering is assumed to be due to a static spherical nuclear charge distribution. Effects due to recoil, inelasticity, and deformation from sphericity are neglected in this work. The calculations have been performed on an IBM 650 calculator employing a modification of a program used previously for obtaining μ meson cross sections and polarizations.[5] The method is very similar to the one used by Yennie, Ravenhall, and Wilson[6] and involves numerically integrating the electron or positron wave function from the origin to a point x_0 outside the nucleus.[7] The phase shifts are obtained by matching the wave functions to the regular and irregular Coulomb wave functions calculated at x_0 by series expansion. Additional details are contained in the work on μ scattering[5] which will be denoted here as I for further references.

The three-parameter charge distribution $\rho(r)$ has the form[8]

$$\rho(r)=\rho_0(1+wr^2/c^2)/\{1+\exp[(r-c)/z]\}, \quad (1)$$

where c and z are constants which determine the halfway radius and the surface thickness, respectively, ρ_0 is a suitable normalization constant such that $4\pi\int_0^\infty\rho(r)r^2dr=Ze$, and w is a third parameter which, when different from zero, produces the "wine-bottle"-like central depression. It should be kept in mind that w in addition increases the value of the charge distribution in the surface region, as becomes apparent in Fig. 6 of Hahn *et al.*[4] or Fig. 3 of this paper. In the case of $w=0$, the surface thickness t, as described by Hofstadter,[2] is equal to $4.40z$, and the halfway radius is given by c. It is also customary to define c_0 by the relation $c=c_0A^{\frac{1}{3}}$.

The choice of the parameters c, z, and w for the cases I to IV presented in Sec. III is suggested by the following considerations.

In the determination of the nuclear charge distribution from the experimental scattering cross sections, the procedure is as follows: A family of radial shapes for the charge distribution is chosen as a function of a number of parameters. Each point in the space of the parameters determines a particular form for the charge distribution and a corresponding theoretical scattering cross section. On account of the experimental error in the cross section, the form of the charge distribution cannot be determined uniquely, giving rise to an "uncertainty region" in the space of the parameters which surrounds the point corresponding to the best fit. That the uncertainty region can be rather extended has been shown by the three-parameter investigation of Hahn *et al.*[4] for the case of 183-Mev electrons scattering on Au, as will be described below.

If positron scattering were simultaneously available, then an additional positron uncertainty region could be established in the space of the charge distribution parameters, and the intersection of the two regions would determine the final uncertainty in the charge distribution. The degree of usefulness of employing positrons in addition to electrons can, therefore, be ascertained from a study of the nature of the overlap of the two regions of uncertainty.

The various choices of shapes of nuclear charge distributions which have been tried in connection with electron scattering have shown[2] that the charge distribution is determined with greatest accuracy in the surface region. In the case of positron scattering, the repulsive nature of the Coulomb interaction leads one to expect that the charge distribution is determined with greatest accuracy in a region somewhat further

[4] B. Hahn, D. G. Ravenhall, and R. Hofstadter, Phys. Rev. **101**, 1131 (1956).

[5] G. H. Rawitscher, Phys. Rev. **112**, 1274 (1958).

[6] D. R. Yennie, D. G. Ravenhall, and R. N. Wilson, Phys. Rev. **95**, 500 (1954).

[7] A list of notations and definitions is given at the end of Sec. I.

[8] This form was first introduced in the work cited in footnote 4, Eq. (8), where it is denoted by "shape (8)" or 3-parameter. In the present paper this nuclear distribution will be denoted by WB whenever $w\neq0$ and WS otherwise. The latter is denoted by EXT in the work cited in footnote 5.

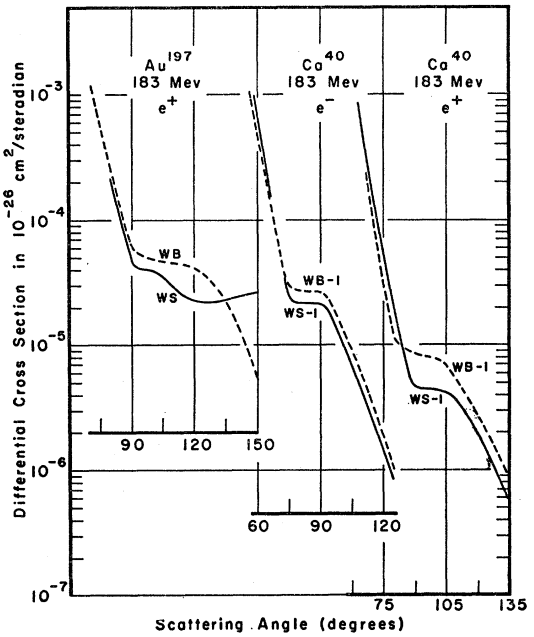

FIG. 1. Comparison of scattering cross sections for various radial nuclear charge distributions. The first pair of curves shows the scattering of 183 Mev positrons on gold. The form of the nuclear charge distribution is given in Eq. (1), text. The values of the parameters are taken from the work cited in footnote 4, Table I. For the curve labeled WS the parameters are $c=6.38$, $z=0.535$, $w=0$; for the curve labeled WB they are $c=6.07$, $z=0.613$, and $w=0.64$. The corresponding electron cross sections are plotted in Fig. 3 of the reference cited in footnote 4, and the nuclear charge distributions are shown in Fig. 6 of the same reference. Numerical uncertainties in the theoretical values are indicated in Fig. 2, where the comparison to the corresponding electron cross section is also illustrated. The other two pairs of curves illustrate the 183-Mev electron and positron cross sections for Ca calculated in connection with case II. The comparison of the cross sections is shown in Fig. 4, where an estimate of the theoretical accuracy is also given. The nuclear charge distributions corresponding to the curves labeled WB–1 and WS–1 are defined in Table I. The dependence of the nuclear charge distribution on the radial distance resembles either a Woods-Saxon shape (WS) or a wine bottle shape (WB).

removed from the center than in the case of electron scattering at the same energy. This expected difference is kept in mind in the present comparison of the electron and positron shape-parameter uncertainty regions, especially for the nuclear surface parameters.

The cases described in Sec. III are intended to throw light on the differences in the positron and electron uncertainty regions in the space of the shape parameters. In particular, cases I and II show that the wine bottle Woods-Saxon ambiguity described by Hahn *et al.*[4] which arises in electron scattering can be reduced by the measurement of positron scattering. Cases III and IV explore the difference of the sensitivity of positrons and electrons to a change in the nuclear surface and interior regions, respectively.

III. CALCULATION

Case I is an extension to positrons of the comparison between wine bottle (WB) and Woods-Saxon (WS) shapes carried out by Hahn *et al.*[4] for 183 Mev electrons scattered by gold. The values of the nuclear shape parameters are taken from Table I of their paper[4] and listed in the caption of Fig. 1. The positron cross sections are shown in Fig. 1. Figure 2 gives the ratio of the electron cross sections corresponding to the two nuclear distributions as well as the ratio for the corresponding positron cross sections. Comparison of the two ratios shows a large difference, mainly in the backward direction. However, the result should only be taken as a qualitative indication of the relative merits of the two particles in view of the numerical uncertainties attached to this particular case. An estimate of these inaccuracies is contained in Sec. IV. All cross-section ratios contained in the shaded area of Fig. 3 have an uncertainty larger than the value of the ratio itself. Cross section ratios at a given angle which are not contained within the shaded area have a numerical uncertainty less than the value indicated by the upper and lower borders of the shaded area at the same angle.

The calculations to be described next refer to 183-Mev electrons and positrons scattered by Ca^{40}. In these cases the accuracy is better than for the case of Au because of the smaller value of the matching radius x_0. This point will be discussed in Sec. IV. On the other hand, due to the smaller values of Z and x_0, the differences between the cross sections corresponding to the various nuclear charge distributions are also less pronounced.

Case II, an extension of case I to the nucleus of Ca, is intended to compare the effectiveness of positrons and electrons in resolving a WS–WB ambiguity. The values of c and z for the Woods-Saxon shape, labeled WS–1, are equal to the ones derived from the electron scattering experiments.[2,4] For the wine-bottle-like distribution, denoted by WB–1, the value of w is taken arbitrarily equal to 0.64, and the values of c and z are

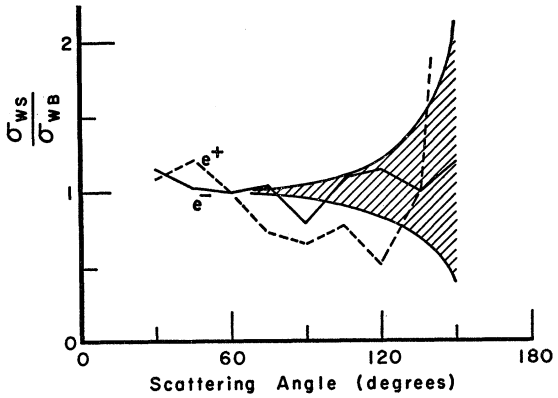

FIG. 2. Comparison of the sensitivity of 183-Mev electron and positron differential scattering cross sections to a change in the radial charge distribution of the Au nucleus. The two distributions are the WB (wine bottle) and WS (Woods-Saxon) defined in the caption to Fig. 1, and described as case I in the text. The ratio of the WS to the WB cross sections is shown by the dashed curve for positrons and by the solid line for electrons. The shaded area shows an estimate of the numerical uncertainty of the cross section ratios as described in the text.

TABLE I. Charge distribution parameters for the nucleus of Ca used for cases II, III, and IV. The parameters are defined in connection with Eq. (1).

Shape	w	c	z	c_0	t
WS–1	0	3.625	0.568	1.060	2.500
WS–2	0	3.625	0.602	1.060	2.650
WB–1	0.64	3.336	0.560	0.976	2.464
WB–2	1.00	3.129	0.570	0.915	2.510

chosen by analogy to the Au case such that the resulting electron cross section is reasonably close to the WS electron cross section. The values of the parameters which define the various charge distributions used for cases II–IV are listed in Table I. In Fig. 3 the nuclear charge distributions for case II are compared. The values of the cross section have already been presented in Fig. 1, and in Fig. 4 their ratios are compared. The shaded area shows the limits of the uncertainty factor up to which the cross section ratios are determined as explained in connection to case I. Comparison of the results shows that positrons are more sensitive than electrons to the change of nuclear charge distribution, the difference in the ratios of cross sections being about a factor of 1.8 near the region of the diffraction dip.[9] From the WS–WB comparisons of cases I and II it cannot be concluded that positrons are better probes of the nuclear interior than electrons are. The reason is that the WS charge distribution differs from that for WB in the surface region as well as inside, as can be seen from the plot of $r^2\rho(r)$ versus r in Fig. 6 of Hahn *et al.*[4] or from the lower half of Fig. 3 of this paper. This observation provides the motivation for the work on case III described below. The lower part of Fig. 3 shows differences of the charge contained within the distance r for the various forms of the charge distributions used in the calculations of cases II to IV. The curves are helpful in the comparison of the small charge distribution differences at large distances, and in addition illustrate a quantity of physical interest which is the charge. For comparison, the quantity which enters the calculation of the potential at distance R is

$$(1/R)\int_0^R r^2\rho dr+\int_R^\infty r\rho dr,$$

showing that $\rho(r)$ does not enter the calculations directly.

Case III. The effect of a 6% change in the surface thickness t on the cross section for a WS nuclear shape is shown in Fig. 5. The more diffuse shape is denoted by WS–2. The dotted curve represents the ratio of the cross sections for positrons, the dash dot curve refers to electrons. With the exception of the point at 165°, the posi-

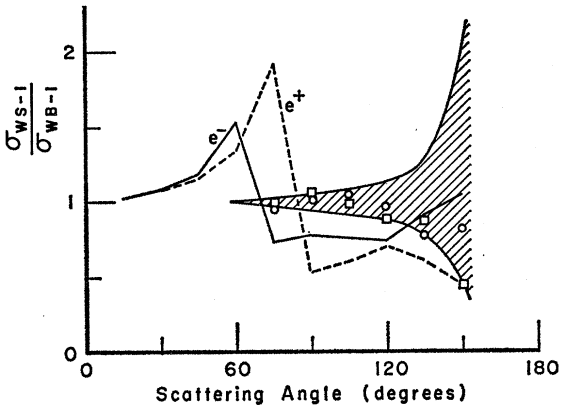

FIG. 4. Comparison of 183-Mev electron and positron cross sections for two nuclear charge distributions of Ca. The distributions are WS–1 and WB–1 defined in Table I and discussed as case II in the text. The ordinate shows the ratio of the cross sections $\sigma_{WS-1}/\sigma_{WB-1}$, the solid curve referring to electrons, the dotted one to positrons. The two curves permit a comparison of the effect on the cross section of a change in the nuclear charge distribution from WS–1 to WB–1, both for electrons and for positrons. The cross section ratios are calculated at the angles 30°, 45°, etc. up to 150° and connected by straight lines. The circles and squares are the results of accuracy tests A and B, respectively, described in Sec. IV. The shaded area indicates an upper limit to the numerical uncertainties, as described in the text.

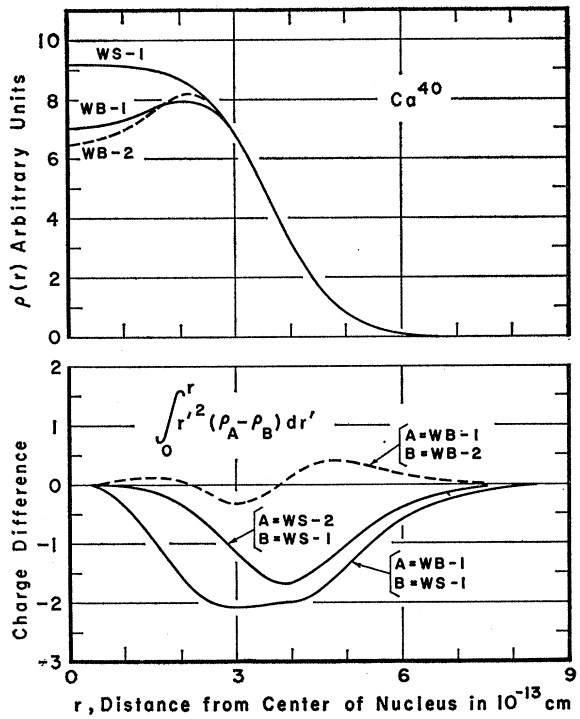

FIG. 3. Charge distributions $\rho(r)$ vs r used in the calculation of cases II to IV. The normalization is such that $\int_0^\infty r^2\rho dr$ is the same for all charge distributions. The various distributions are defined by Eq. (1) with the parameters given in Table I. Differences between the charge distributions for large r are too small to be apparent from the plot of $\rho(r)$ vs r. These differences are illustrated in the lower part of the figure by means of plots of the difference for two distributions of the charge $\int_0^r r'^2\rho dr'$ contained within the radius r. The ordinate is in arbitrary units.

[9] A more accurate search for the WB shape parameters such that the WS and WB electron cross section difference is minimized does not seem warranted in the present preliminary investigation.

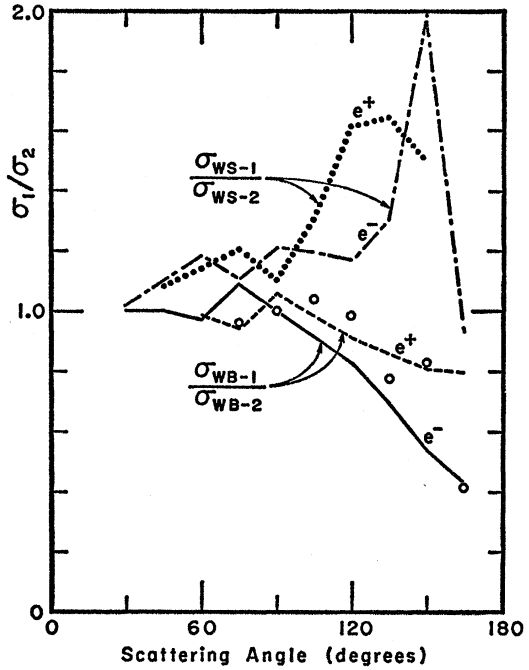

FIG. 5. Comparison of the effect on the scattering cross section of a change in the interior region of the nuclear charge distribution of Ca^{40} to a change at the surface. The upper two curves show the ratio of the cross sections for two WS charge distributions which differ by 6% in the surface thickness, described as case III in the text, and defined in Table I. Here the ordinate σ_1/σ_2 represents the ratio $\sigma_{WS-1}/\sigma_{WS-2}$, where WS-2 has the larger surface thickness. The dotted line is for positrons, the dot dash curve corresponds to electrons. The lower two curves, described in the text as case IV, correspond to a change of the interior of the nucleus. In this case the ordinate σ_1/σ_2 represents the ratio of the differential cross sections for charge distributions WB-1 and WB-2, defined in Table I and illustrated in Fig. 3. The dashed curve is for positrons, the solid line refers to electrons. The cross section ratios are calculated at the angles 30°, 45°, etc., and connected by straight lines. The circles represent the results of the numerical uncertainty test *A* described in Sec. IV.

tron cross sections appear to be more affected by the nuclear surface change than the electron cross sections.

For case IV a distribution WB–2 is selected which differs from WB–1 mainly in the central nuclear region, as is illustrated in Fig. 3. The ratios for the two distributions of the positron and electron cross sections are illustrated in Fig. 5. Comparison of the two ratios shows that a change from WB–1 to WB–2 in the nuclear charge distribution changes the electron cross section at least as much as it does the positron cross section. It is very likely that electrons are more effective than positrons in "seeing" the inside of the nucleus. This conclusion, although suggested by the results of case IV, is not definitely shown here because of the lack of accuracy of these results.

IV. ACCURACY ESTIMATES

The numerical errors in the calculation of the Coulomb and nuclear wave functions at the matching point will be investigated in some detail in this section. The accuracy of the wave function determines to a large extent the accuracy of the nuclear phase shift and hence that of the cross section, as discussed in the following.

Outside of the nuclear region the potential is Coulomb and the nuclear radial wave functions[10] G_k and F_k can be expressed as linear combinations of the regular and irregular Coulomb wave functions through the relations[7]

$$\begin{aligned} G_k &= C_k G_k{}^R + D_k G_k{}^I, \\ F_k &= C_k F_k{}^R + D_k F_k{}^I. \end{aligned} \tag{2}$$

The functions G, F, G^R, F^R, G^I, and F^I are defined in Eqs. (A1) to (A5) of the Appendix, where a connection to the quantities numerically calculated is also given. The point beyond which the charge distribution is neglected in the numerical calculations is denoted by x_0 and will be referred to as the matching point. For each k the effects of the nuclear charge distribution enters the calculation of the nuclear phase shift δ_k only through the ratio D_k/C_k, as is shown by Eq. (A15). The calculation of D_k/C_k in terms of the radial wave functions involves the combination

$$G_k{}^R - F_k{}^R(G_k/F_k) \tag{3}$$

as can be seen for instance from Eq. (9A) of I.[5] For a given accuracy in the radial wave functions the accuracy obtained for the nuclear phase shift depends on the degree of cancellation between the two terms in expression (3).[11]

An indication of the cancellation per unit nuclear phase shift can be obtained from the quantity

$$\frac{G^R - F^R(G/F)}{\frac{1}{2}[G^R + F^R(G/F)]} \Big/ [\tan(\sigma^R+\delta) - \tan(\sigma^R)] = Q. \tag{4}$$

Here the subscripts k have been suppressed. For the calculations of cases II to IV, x_0 was near 7.7 and near 8.7 for test case *B*. The values k in these calculations, for which the nuclear phase shift is nonnegligible, run from ± 1 to ± 8. For k larger than 4 the nuclear phase shift is less than 10^{-2} rad. Values of Q as a function of x_0 have been obtained for the sample cases $k=\pm 1$ and $k=\pm 6$ for 183 Mev electrons and positrons scattering on form WS–1 of Ca^{40}. Use was made of expression (A14) which is a good approximation to Q in this case. For $k=\pm 1$, Q is above 2 in the vicinity of $x_0=8$ for both electrons and positrons. For $k=\pm 6$, Q goes through a minimum near $x_0=7.8$, where its value is close to 0.7. No particularly troublesome cancellations are, therefore, to be expected in the calculations, other than the cancellations which naturally occur whenever the nuclear phase shifts are small. For example, for a nuclear phase shift δ_6 of 10^{-2} rad, the cancellation in the expression (3)

[10] G. Breit and G. E. Brown, Phys. Rev. **76**, 1307 (1949).

[11] The additional quantity $(G/F)F^I - G^I$ enters in the calculation of D_k/C_k in terms of the wave functions. For the case of interest, for which the nuclear phase shift is small, cancellations in the above quantity are small compared to the cancellation in expression (3) and will not be considered here.

will occur in the first two significant figures, indicating that an accuracy of better than 0.1% is required in the knowledge of the wave functions in order to obtain an accuracy of 10% for the nuclear phase shift.

The Coulomb wave functions are calculated at the matching point by a power series expansion in x_0, using the expression (11A) of I.[5] Since the coefficients in the expansion are related by recurrence relations, numerical errors can accumulate and increase as the number of terms in the summation increases, as is the case when the value of x_0 increases.

Two tests have been performed in order to estimate the accuracy in the calculations of the cross sections of cases II and IV. Both tests have been done for 183 Mev electrons and the WS–1 charge distribution of the nucleus of Ca. The matching point for this case has a value close to 7.70.

In test A the precision of the Coulomb and nuclear wave functions is estimated, and the resulting precision in the differential cross section is calculated. The procedure is as follows. Electron regular and irregular Coulomb wave functions are computed by series expansion at x close to 1.7, where the accuracy is expected to be better than at 7.7 on account of the smaller number of terms required in the expansion. If these wave functions were now numerically integrated out to $x_0=7.7$ and then compared to the Coulomb wave functions calculated by series expansion at that point, an estimate of the error would be obtained. However, in order to avoid possible initial condition errors due to the increasing or decreasing nature of the particular regular and irregular Coulomb wave functions in the interval $1.7<x<7.7$, a combination of these functions is utilized instead. The combinations are of the type indicated by Eq. (2), with the coefficients C_k and D_k taken equal to those occurring in the calculation of case II, electrons, WS–1. The ratio of the wave functions at $x=7.7$ obtained in this manner by integration started at 1.7 is labeled $(G/F)_{\text{Int}}$; the corresponding ratio obtained by using the same combination of Coulomb wave functions calculated by series expansion at $x=7.7$ is labeled $(G/F)_{\Sigma}$. The numerical integration is done by the same method as the one used in the calculation of the nuclear wave functions, as described in I,[5] and the integration interval is varied until the integration error is definitely smaller than the difference to be measured. The expression

$$[(G/F)_{\Sigma}-(G/F)_{\text{Int}}]/(G/F)_{\text{Int}} \qquad (5)$$

is found to be less than 2×10^{-5} for $k=\pm1$ and ±6, indicating that the error in the ratio of Coulomb wave functions is less than $10^{-2}\%$.

From the variation of the integration interval, the error in the nuclear wave function ratios as calculated in cases II to IV is estimated to be less than $10^{-3}\%$ and, therefore, each term in the expression (3) should have an error of less than $10^{-2}\%$. For the purpose of test A, a change of about $10^{-2}\%$ is deliberately introduced into the regular and irregular Coulomb wave functions at the matching point by replacing the sixth, seventh, and eighth significant figures by zeros. The cross section resulting from these modified wave functions is recalculated and the ratio of the cross section thus obtained to the original one,

$$(d\sigma/d\Omega)_{\text{Test}}/(d\sigma/d\Omega),$$

is represented by circles in Figs. 4 and 5.

In test B the matching point is changed from the original value close to 7.7 to the value 8.7, and the cross section is recalculated without further alterations. Care is taken that all nuclear charge lies within the original x_0 also in this case. The ratio of new to old cross sections is shown by the squares in Fig. 4. The merit of this test is that no artificial conditions are introduced. On the other hand, test B is possibly too severe because of the large value of the matching distance which increases the error in the Coulomb wave functions to a value greater than what it presumably is in the calculations of cases II to IV.

The shaded area shown in Fig. 4 is obtained by plotting the inverse of the cross section ratios of tests A and B, in addition to the direct ratios, and then drawing smooth upper and lower limiting curves. The shaded area shown in Fig. 2 is obtained in a similar fashion, based on a test A done in this case for 183-Mev electrons scattering on the WS distribution of the gold nucleus.

V. SUMMARY AND CONCLUSIONS

A comparison between electrons and positrons as tools for determining the radial dependence of the nuclear charge density has been undertaken by means of a few exploratory sample calculations.

The method consists in varying the shape of the radial dependence of the nuclear charge distribution as determined by three parameters, and numerically calculating the scattering cross sections for both positrons and electrons for each shape. The nuclei studied are Ca^{40} and Au^{197} at 183-Mev incident energy.

A comparison of the results indicates that positron cross sections are affected differently than electron cross sections for a given change in the nuclear charge distribution[12] by as much as a factor of 2 in the case of Au and by a factor of about 1.5 in the case of Ca for one of the examples studied. Indications exist that positrons are more affected than electrons by a change of the charge distribution at the nuclear surface. It is felt that additional investigation of the difference between electrons and positrons, as well as μ mesons, in their ability to serve as nuclear probes, would be warranted.

[12] Equation (A7) of the Appendix expresses the change in phase shift produced by a change in potential $\bar{V}-V$ in terms of an integral of $\bar{V}-V$ over the interior of the nucleus. The weighting factor is the combination $\bar{F}F+\bar{G}G$ which depends on whether the potential V is attractive or repulsive.

ACKNOWLEDGMENTS

The authors wish to thank Professor Gregory Breit for the interest with which he accompanied the various phases of this work, for the many helpful suggestions given to them, and for a critical reading of the manuscript. In addition, they would like to acknowledge the computing time provided to them at New Mexico State University by the IBM Corporation.

APPENDIX

The functions[13] $F_k(r)$ and $G_k(r)$ are equal to r times the corresponding radial wave functions and satisfy the equations,

$$\begin{aligned}(1/\hbar c)(E+mc^2-V)F_k-(d/dr+k/r)G_k=0,\\(1/\hbar c)(E-mc^2-V)G_k+(d/dr-k/r)F_k=0,\end{aligned}\tag{A1}$$

where E and m are, respectively, the total energy and rest mass of the incident particle, V is the electrostatic potential due to the nuclear charge distribution, and k is defined at the end of Sec. I.

The normalization is such that asymptotically

$$\begin{aligned}G_k&\sim\sin\varphi_k,\\F_k&\sim[(E-mc^2)/(E+mc^2)]^{\frac{1}{2}}\cos\varphi_k,\end{aligned}\tag{A2}$$

where φ_k is defined below.

In the point nucleus case, V is the Coulomb potential and[7]

$$\begin{aligned}\varphi_k{}^S&=x-k\pi/2-\eta\ln 2x+\sigma_k{}^S, && k>0\\&=x-(|k|-1)\pi/2-\eta\ln 2x+\sigma_k{}^S, && k<0.\end{aligned}\tag{A3}$$

Here the superscript S stands for either R or I according to whether the quantities so labeled refer to the regular or irregular Coulomb wave functions, respectively. For example, $\sigma_k{}^R$ is the relativistic equivalent of the quantity σ_L, usually denoted as the Coulomb phase shift, where $L=|k|-1$. The right-hand side of Eq. (A6) of I[5] gives an expression for both $\sigma_k{}^R$ and $\sigma_k{}^I$, where they are denoted by $\eta_{-k}{}^R$ and $\eta_{-k}{}^I$. The irregular Coulomb wave function used in this work is defined, in analogy to the regular function, in terms of a power series expansion given by Eq. (11A) of I[5] together with Eq. (A5) of this paper. As a result, unlike the nonrelativistic case, $\sigma_k{}^I$ and $\sigma_k{}^R$ do not differ by $\pi/2$.

In the case that V corresponds to an extended nuclear charge distribution, the nuclear wave functions F_k and G_k are regular at the origin and satisfy relations (A1) and (A2). In this case the asymptotic phase φ_k differs from $\varphi_k{}^R$ by the nuclear phase shift δ_k

$$\varphi_k=\varphi_k{}^R+\delta_k.\tag{A3'}$$

The functions F_k and G_k are related to the functions $\mathfrak{F}_{-k}$ and $\mathfrak{G}_{-k}$ of I[5] by the equations[14]

$$\begin{aligned}G_k&=[(E/mc^2)+1]^{\frac{1}{2}}\mathfrak{G}_{-k},\\F_k&=-[(E/mc^2)-1]^{\frac{1}{2}}\mathfrak{F}_{-k}.\end{aligned}\tag{A4}$$

The nuclear wave functions $\mathfrak{G}_k$ and $\mathfrak{F}_k$ are calculated by means of numerical integration of Eqs. (2A) of I.[5] The Coulomb wave functions $\mathfrak{G}_k{}'^R$, $\mathfrak{G}_k{}'^I$, $\mathfrak{F}_k{}'^R$ and $\mathfrak{F}_k{}'^I$ of I are the quantities numerically calculated by series expansion. They are related to the unprimed quantities by the expressions

$$\begin{aligned}\mathfrak{G}_k{}^S&=[(E/mc^2)+1]^{-\frac{1}{2}}N_k{}^S x_0{}^{s(k)}\mathfrak{G}_k{}'^S,\\\mathfrak{F}_k{}^S&=[(E/mc^2)+1]^{-\frac{1}{2}}N_k{}^S x_0{}^{s(k)}\mathfrak{F}_k{}'^S.\end{aligned}\tag{A5}$$

Here the superscript S stands for either R or I and

$$s(k)=\pm(k^2-Z^2\alpha^2)^{\frac{1}{2}},$$

the $+$ and $-$ signs corresponding, respectively, to the regular and irregular cases. The normalization coefficients $N_k{}^S$ are given by Eq. (13A) of I.[5] The definition of G and F used in this work, Eqs. (A1) and (A2), is along the lines of Breit and Brown,[10] lends itself better for the passage to the nonrelativistic case, and is more useful for the derivations to be given below. The mass, although negligible for the application to positrons and electrons, is kept in the formulas for the sake of completeness.

It will now be shown how

$$G_k{}^I F_k{}^R-G_k{}^R F_k{}^I=[(E-mc^2)/(E+mc^2)]^{\frac{1}{2}}\times\sin(\sigma_k{}^I-\sigma_k{}^R),\tag{A6}$$

$$\sin(\bar{\delta}_k-\delta_k)=-[(E+mc^2)/p^2c^2]\times\int_0^\infty(\bar{G}_kG_k+\bar{F}_kF_k)(\bar{V}-V)dx,\tag{A7}$$

can be derived. These relations have been found useful in checking the numerical work and also as partial indicators of the accuracy of the numerical methods used. Here $\bar{G}_k$ and $\bar{F}_k$ are defined by Eqs. (A1) and (A2), with the potential given by $\bar{V}$, while the potential corresponding to G_k and F_k is V. By defining the column vectors

$$\chi=\begin{pmatrix}F_k\\G_k\end{pmatrix},\quad\bar{\chi}=\begin{pmatrix}\bar{F}_k\\\bar{G}_k\end{pmatrix},\tag{A8}$$

[13] The notation and use of the wave functions is along the lines of the work cited in footnote 10. The authors are grateful to Professor G. Breit for pointing out to them a simplification in the original proof of Eqs. (A6) and (A7).

[14] A misprint occurred in Eqs. (1A) of I. The correct relations are

$$\begin{aligned}G_k&=r^{-1}(E+1)^{\frac{1}{2}}\mathfrak{G}_k,\\F_k&=r^{-1}(E-1)^{\frac{1}{2}}\mathfrak{F}_k.\end{aligned}$$

The function G and F of I should not be confused with the functions denoted by the same symbols in the present work. In addition, the quantity $\gamma\ln 2x$ should be added to the expression in square brackets of Eqs. (4A) of I.

and the matrices

$$P=\begin{pmatrix}(1/\hbar)(p+mc) & -k/r\\ -k/r & (1/\hbar)(p-mc)\end{pmatrix},$$
$$\epsilon=\begin{pmatrix}0 & -1\\ 1 & 0\end{pmatrix},\quad I=\begin{pmatrix}1 & 0\\ 0 & 1\end{pmatrix}, \tag{A9}$$

where $p=(E-V)/c$ and $\bar{p}=(\bar{E}-\bar{V})/c$, the Eqs. (A1) can be written

$$(P+\epsilon d/dr)\chi=0, \tag{A10}$$

$$\bar{\chi}^T\bar{P}^T+(d/dr)\bar{\chi}^T\epsilon^T=0, \tag{A11}$$

where the superscript T indicates transposition. By multiplying Eq. (A10) on the left by $\bar{\chi}^T$ and Eq. (A11) on the right by χ, subtracting, and remembering that $\epsilon^T=-\epsilon$, one obtains

$$d(\bar{\chi}^T\epsilon\chi)/dr=\bar{\chi}^T(P-\bar{P}^T)\chi. \tag{A12}$$

If $V=\bar{V}$ and $E=\bar{E}$, then $P=\bar{P}=\bar{P}^T$ and the right-hand side of Eq. (A12) vanishes. The left-hand side is the derivative of $\bar{G}_kF_k-\bar{F}_kG_k$, which, therefore, is a constant. By specializing to the Coulomb case, referring to regular and irregular wave functions by symbols without and with bars, respectively, and by making use of the asymptotic relations (A2) and (A3), Eq. (A6) is obtained.

If $V\neq\bar{V}$ and $E=\bar{E}$, then

$$\bar{P}^T-P=(1/\hbar)(-\bar{V}+V)I.$$

By integrating both sides of Eq. (A12) over dx from 0 to ∞, one obtains

$$(\bar{G}_kF_k-\bar{F}_kG_k)\Big|_0^\infty = -(1/pc)\int_0^\infty(\bar{F}_kF_k+\bar{G}_kG_k)(\bar{V}-V)dx.$$

The left-hand side vanishes at $x=0$, and making use of Eqs. (A2), (A3) and (A3′) at $x=\infty$, relation (A7) results. For computational purposes, a useful form of Eq. (A6) in terms of the functions $\mathfrak{F}_k'^S$, $\mathfrak{G}_k'^S$ defined by the relations (A5) is the following:

$$\mathfrak{G}_k'^R\mathfrak{F}_k'^I-\mathfrak{G}_k'^I\mathfrak{F}_k'^R = -2(k^2-Z^2\alpha^2)^{\frac{1}{2}}\eta[(1-\beta^2)^{\frac{1}{2}}+1]/(Z^2\alpha^2). \tag{A13}$$

An approximate expression for Q, defined in Eq. (4) of the text, is as follows

$$Q_k\approx-\tfrac{1}{2}[G_k^R]^{-1} \times[(E+mc^2)^{\frac{1}{2}}(E-mc^2)^{-\frac{1}{2}}F_k^R]^{-1}\cos^2\sigma^R. \tag{A14}$$

For simplicity the indices k are left out in what follows. To prove the result, use is made of the relation

$$\tan(\sigma^R+\delta)-\tan\sigma^R = \frac{D/C}{1+(D/C)(\cos\sigma^I/\cos\sigma^R)}\frac{\sin(\sigma^I-\sigma^R)}{\cos^2\sigma^R}, \tag{A15}$$

which is equivalent to Eq. (5A) of I.[5] Making use of relation (2), one finds

$$\frac{G^R-F^R(G/F)}{G^R+F^R(G/F)}=\frac{G^RF^I-F^RG^I}{2(C/D)G^RF^R+(G^RF^I+G^IF^R)},$$

In the cases discussed in the text and where the cancellations in expression 3 are of importance, δ and hence D/C is small compared to 1, and $G^RF^I+G^IF^R$ can be neglected with respect to the term in C/D. Neglecting, in addition, the term in D/C in the denominator of the right hand side of Eq. (A15) and making use of expression (A6), the result (A14) follows. In case of zeros in either G^R or F^R, the approximations leading to Eq. (A14) are not valid.